



AIAA 98-0330

Scaling of an Oscillatory Flow
Control Actuator

J.T. Lachowicz, C.-S. Yao, and R.W. Wlezien
NASA Langley Research Center
Hampton, VA

**36th Aerospace Sciences
Meeting & Exhibit**
January 12-15, 1998 / Reno, NV

SCALING OF AN OSCILLATORY FLOW-CONTROL ACTUATOR

Jason T. Lachowicz*, Chung-Sheng Yao† and Richard W. Wlezien‡
 NASA Langley Research Center, Hampton, VA 23681

Abstract

An oscillatory flow control actuator is characterized in still air using flow visualization and mean velocity measurements. The actuator produces flow in several regimes that may be used for active flow control. The non-dimensional scaling for each flow regime is developed. The scaling is general and may be applied to the design of other oscillatory flow control actuators (such as vortex generator jets or synthetic jets) by an appropriate interpretation of the non-dimensional variables. The oscillatory flow control actuator generates a free jet, wall jet, vortex flow, or a combination of these flows depending on the scaling parameters. For the vortex flow field, the actuator operational range increases as the actuator size decreases, which may facilitate micro-actuator design. The optimum actuator efficiency occurs at a Stokes number of about 8 for the vortex flow.

Nomenclature

a	Actuator amplitude (mm)
b	Actuator width (mm)
f	Actuator frequency (Hz)
g_n	Ratio of narrow gap width to actuator width
g_w	Ratio of wide gap width to actuator width
g_r	Ratio of g_w to a reference g_w of 0.033
Re	Actuator Reynolds number = $U b/\nu$
S_a	Scaled amplitude = $2 \pi a/b$
St_n	Stokes number at narrow gap = $(2 \pi f w_n^2/\nu)^{1/2}$
St_w	Stokes number at wide gap = $(2 \pi f w_w^2/\nu)^{1/2}$
U_p	Actuator peak velocity = $2 \pi a f$ (m/s)
U	Horizontal velocity component (m/s)
U_o	Horizontal velocity at $x=1$ mm
V_w	Theoretical vertical velocity from the wide gap, $V_w = U_p b/w_w$
w_n	Narrow gap width (mm)
w_w	Wide gap width (mm)
ν	Kinematic viscosity (m^2/s)
x	Distance along the actuator width measured from the wide gap edge of the actuator
y	Distance perpendicular to the actuator

Introduction

Flow control techniques for improving aircraft performance have been predominately passive. These techniques are characterized by fixed devices that are configured to improve system performance. An example of a passive separation control device is a fixed vortex generator¹⁻³ used on high-lift systems. At landing/takeoff conditions, the vortex generator transports high-momentum fluid from the outer boundary layer towards the wing surface, energizing the boundary layer and delaying separation. Thus, lift is increased and performance losses are reduced. Though these devices are simple, rugged, and relatively low in cost, there are two significant disadvantages: i) passive devices cannot be controlled, e.g. for landing/takeoff flight or maneuvering flight; and ii) passive control devices add parasitic drag in situations where stall suppression is not needed, e.g. steady, cruise conditions.

Active techniques⁴⁻¹² have the potential to minimize both disadvantages while optimizing overall performance. For example, an active counterpart of a conventional vortex generator is the vortex-generator-jet⁴⁻⁷ (VGJ). Unlike vortex generators, which control separation¹⁰ only during aircraft takeoff and approach, the VGJ can be optimized at off-design conditions to enable separation control when necessary. Also, the drag penalty of the VGJ is negligible when the jets are turned off. The oscillatory flow-control actuator of this study also shares these same advantages and may be used for similar applications. However, unlike VGJs, no external plumbing is required, allowing for reduced vehicle mass and design simplicity. In addition, the oscillatory actuator operates over a range of amplitudes and frequencies, potentially allowing control over different flight regimes.

The primary goal of active techniques is to develop efficient actuators that can be integrated with flight control systems to enable longer aircraft range, maneuverability, and stability. Most of the focus has been on surface mounted actuators that either reduce drag, enhance lift, or produce a controlled force vector about some axis of the aircraft. The present study also focuses on surface mounted actuators. However, unlike more conventional systems which extract energy from the mean flow field, the present actuator system is designed to produce vorticity from the actuator itself.

Originally, Jacobson and Reynolds¹⁴ studied an oscillatory flow control type actuator (2.5 mm x 20 mm) in water at 0.25 m/s and at an amplitude and frequency of 0.13 mm and 330 Hz, respectively. The actuator was flush-mounted along a flat plate model and was placed

*NRC Post-Doctoral Research Associate, Member AIAA

†Senior Research Scientist, Member AIAA

‡Senior Research Scientist, Associate Fellow AIAA

This paper is declared a work of the US Government and is not subject to copyright protection in the United States.

asymmetrically forming wide and narrow gaps when viewed from the top of the plate. A periodic emerging jet on the narrow gap side induced longitudinal vorticity within the flat plate boundary layer. The actuators were integrated with wall shear sensor arrays in order to actively control transitional boundary layers.

Saddoughi¹⁵ increased the actuator size an order of magnitude (28 mm x 250 mm) to use the system as an active separation control actuator. The actuators were tested in air up to 5 m/s and at an amplitude and frequency of 10 mm and 50 Hz, respectively. Under these conditions, the actuator produced a jet from the wide gap side of the actuator.

Both experimental configurations were studied numerically by Koumoutsakos^{16,17} using direct numerical simulations of the control actuator with no external flow. These studies showed that at relatively low amplitudes and high frequencies, the periodic jet develops from the narrow gap, and at relatively high amplitudes and low frequencies, the periodic jet develops from the wide gap. These results are consistent with the experiments^{14,15}.

The primary objectives of the present research are to examine the oscillatory flow control actuator without external flow in order to develop the non-dimensional scaling of the system, and to understand the flow field characteristics. The scaling laws can subsequently be used to design actuators¹³ suitable for aircraft applications. In general, the approach used in this study may be applied to other flow control actuators.

Experimental Apparatus & Approach

Flow Control Actuator

The experimental configuration of the flow control actuator is illustrated in Fig. 1. The actuator consists of a cavity with a graphite-epoxy composite plate which serves as the actuation surface. A shaker is used to actuate the system in an oscillatory motion. The surface acts like a piston pumping air out of the cavity on the down-stroke and sucking air into the cavity on the upstroke. The actuator is placed asymmetrically over the cavity opening, forming narrow and wide gaps when viewed from the top as shown in Fig. 1.

Flow Control Actuator Scaling

The flow from the actuation system depends on 7 parameters: i) actuator amplitude, a ; ii) actuator frequency, f ; iii) characteristic velocity, U_c ; iv) wide gap spacing, w_w ; v) narrow gap spacing, w_n ; vi) actuator width, b , and vii) kinematic viscosity, ν . According to the Buckingham-Pi Theorem¹⁸, 5 non-dimensional parameters govern the actuator flow field, since these parameters depend on only 2 fundamental dimensions (length & time). An analysis was implemented to provide these 5 non-dimensional parameters:

$$\begin{aligned}\pi_1 &= U_c b / \nu \\ \pi_2 &= U_c / (b f) \\ \pi_3 &= a / b \\ \pi_4 &= w_n / b \\ \pi_5 &= w_w / b\end{aligned}$$

If the actuator peak velocity, $U_p = 2 \pi a f$, is used for the characteristic velocity, then π_2 and π_3 contain the same functional dependence reducing the number of non-dimensional parameters to 4:

$$\begin{aligned}\pi_1 &= Re = U_c b / \nu = 2 \pi f a b / \nu \\ \pi_3 &\propto \pi_2 = S_a = 2 \pi a / b \\ \pi_4 &= g_n = w_n / b \\ \pi_5 &= g_w = w_w / b\end{aligned}$$

Re , S_a , & g_w are written in compact form using the Stokes number¹⁹ at the wide gap:

$$St_w = (2 \pi f w_w^2 / \nu)^{1/2} = (2 \pi Re g_w^2 / S_a)^{1/2} \quad (1)$$

Similarly, Re , S_a , & g_n are written in compact form using the Stokes number at the narrow gap:

$$St_n = (2 \pi f w_n^2 / \nu)^{1/2} = (2 \pi Re g_n^2 / S_a)^{1/2} \quad (2)$$

In this study, w_n is fixed so that only 3 independent parameters are varied: g_w , Re , and S_a . Depending on the non-dimensional parameter range, several flow regimes are produced by the actuator. This paper outlines the ranges over which these flows are obtained.

Measurements

Three primary measurements were used to study the actuator dependent flow field: i) laser-sheet flow visualization; ii) actuator displacement amplitude measurements; and iii) laser velocimetry (LV) measurements.

The flow visualization and actuator amplitude measurements were conducted simultaneously to document the actuator flow field. The laser-sheet flow visualization measurements were conducted in still air using a 3 Watt argon-ion laser and a Pulnix progressive scan camera. The camera provided high resolution images at high shutter speeds (up to 1/16000 sec) and was reset asynchronously to provide both instantaneous and mean flow field pictures. The actuator amplitude was measured using a Philtec fiber-optic displacement sensor (accurate to within ± 0.01 mm). The sensor was also used to monitor the actuator motion throughout testing.

A 2-component LV system was used for point velocity measurements of the actuator flow field. Particles on the order of 1 micron were used for seeding. The LV probe was scanned in several cross-planes (front view of Fig. 1) to provide mean velocity vector measurements and an estimate of the mean vorticity. The LV velocity measurements are accurate to within ± 0.01 m/s.

The actuator flow field was mapped over the operational range of the shaker-actuated flow control system: i) $30 < f < 290$ Hz; and ii) $0.1 < a < 1.1$ mm. The flow regimes were documented using flow visualization and actuator amplitude and frequency measurements. Velocity measurements were then obtained at several locations along the actuator using the LV system.

Results

All results were obtained at a fixed narrow gap width, w_n , of approximately 0.14 mm.

Flow Field Visualization

The primary flow regimes are presented in Figures 2-6 for a fixed actuator width of 9.65 mm. Similar flow fields were observed for all additional actuator widths tested. The camera shutter was set open to capture time averaged flow patterns.

The free jet flow fields are presented in Figs. 2-3 at $g_r = 3$. At relatively low amplitudes, a , the jet is angled as shown in Fig. 2. Near the actuator surface, more fluid moves from the narrow to wide gap. By continuity, fluid must return to the narrow gap side producing the angled jet at the wide gap. As amplitude increases the flow near the actuator surface becomes secondary and the jet is vertical, as shown in Fig. 3.

The wall jet is illustrated in Fig. 4 at $g_r = 3$. The wall jet is primarily horizontal to the right of the narrow gap as indicated by the arrows and is characterized by steady horizontal flow pumping from the wide gap end to the narrow gap end. Thus, the actuator may potentially be used to energize a boundary layer by accelerating the fluid tangentially near the wall surface. This application represents an improvement over conventional tangential blowing methods in regions of large curvature.

As the amplitude is increased from the wall jet regime, a vortex is generated at the wide gap as illustrated in Fig. 5 at $g_r = 3$. The vortex regime may be used to promote mixing and suppress boundary layer separation. This regime may thus be used as an active counterpart to the conventional vortex generator.

As the wide gap is increased, $g_w = 5$, an additional flow regime is produced as shown in Fig. 6. (Note that this flow is also present at very small wide gap widths as illustrated in Fig. 7). This regime represents a free jet emanating from the narrow gap of the actuator. Thus, the actuator may be operated to produce a free jet at either the wide or narrow gaps, depending on the actuator amplitude and frequency.

Flow Field Scaling

The non-dimensional scaling for each of the flows shown in Figs. 2-6 are presented in Figs. 7-16. In each figure, the broken line indicates a low-frequency boundary not surveyed, and the solid line indicates an unsteady flow regime. Data are presented for two actuator widths: $b = 9.65$ & 18.8 mm. Note that the S_a , Re ranges are different for each actuator width case.

Figs. 7 & 10 present the scaling at $g_r = 1$. The flows of interest occur at low actuator Reynolds numbers, $Re < 250$. For both actuator widths, the largest flow regime is the wide gap free jet. A narrow gap free jet also exists for the smaller actuator width case as shown in Fig. 7. The relative range of S_a -values for these 2 free jet flow regimes (wide & narrow) is governed by the Stokes number¹⁹. Equations 1 & 2 show that the Stokes number is proportional to $g_w(Re/S_a)^{1/2}$ or $g_n(Re/S_a)^{1/2}$ for the wide and narrow gaps, respectively. As shown in Fig. 7, the Re -range for both the narrow and wide free jets is approximately the same. Thus, according to Equation 1, for a fixed Re and Stokes number, a larger gap spacing (wide gap), g_w , corresponds to a larger S_a . Similarly, according to Equation 2, for a fixed Re and Stokes

number, a smaller gap spacing (narrow gap), g_n , corresponds to a smaller S_a . Both of these trends verify the results shown in Fig. 7. For the data in Fig. 7, the wide-to-narrow gap spacing is approximately 2.3 corresponding to a S_a ratio of approximately 5, according to equations 1 & 2. As shown in Fig. 7, the S_a -range for the wide gap jet occurs at approximately 5 times the S_a -range for the narrow gap as predicted by the Stokes number scaling. The data of Figs. 7 & 10 also show that the flow regimes are not similar at a fixed g_r . This suggests that the flow type depends strongly on the actuator width. In summary, the Stokes number scaling predicts the relative S_a -range for the narrow and wide gap free jets, and the flow regimes depend strongly on actuator width.

The wide gap spacing is increased in Figs. 8-13 & 16 for 2 different actuator widths. Again, the flow regimes are not similar at a fixed g_r but vary strongly with the actuator width (compare Figs. 8 & 11, 9 & 12, and 13 & 16). As the wide gap spacing increases, $g_w = 5$, the narrow gap free jet flow reemerges and an additional flow field, reverse horizontal flow, appears. The reverse wall jet represents steady horizontal flow pumping from the narrow gap towards the wide gap. LV measurements indicate that the horizontal velocity, 1.5 m/s, near the actuator surface compares within 5% of the values measured for the horizontal flow field.

At larger gap widths, $g_w = 8$, the narrow gap flow field becomes significant as suggested in Fig. 14, where the wide gap free jet is not present and the narrow gap free jet extends over a relatively large S_a , Re regime. The wall jet regimes also extend over a larger range when compared to the smaller gap widths. Overall, the flow regime boundaries for each flow field are well defined and distinct at the larger g_r (i.e. larger gap widths).

Unlike the distinct flow boundaries of Fig. 14, at very small gap widths, $g_r = 1.5$, the flow regime boundaries are interconnected as shown in Fig. 15. The vortex and wall jet flows merge into the free jet flows as S_a is increased (amplitude increased), and the wide-gap free jet dominates. These results suggest that the wide gap jet will span the largest range in (S_a, Re) space as g_r asymptotically approaches zero.

Flow Field Characteristics

The previous section outlined the overall trends associated with increasing g_r at a fixed actuator width. Fig. 9 illustrates the typical trends associated with a fixed g_r . Consider a vertical line at $Re = 50$, which represents a typical low frequency. At low amplitudes (i.e. low S_a), the wall jet exists. As amplitude is increased at this low frequency, the wall jet first develops into the angled free jet and then develops into the vertical free jet at the largest amplitudes. Consider a vertical line at $Re = 150$, which represents a typical large frequency. Similar to the low frequency case, at low amplitudes but high frequency, the wall jet exists. As amplitude is increased the wall jet develops into the vortex flow field. Finally, at the largest amplitudes, the vortex flow develops into an unsteady flow.

Vortex Flow Field

Velocity vectors of the mean flow field are presented in Fig. 17 where the gray rectangle represents the actuator which oscillates in the vertical direction, and the black border represents the cavity. Data were surveyed over the range, $(x,y)=(0-5,2.1-5.08)$ mm, using spacings of 0.5 and 0.42 mm, for x and y , respectively. (Both horizontal and vertical velocity components could not be measured below $y=2.12$ mm due to constraints on the LV measurement volume.) For the range presented, the maximum mean velocity is approximately 1.5 m/s at $(x,y)=(0, 2.12)$ mm. The jet velocities are expected to increase by a factor of 2-3 closer to the actuator. The velocity vectors suggest that the flow is dominated by a clockwise vortex centered at approximately $(x,y)=(1.5,3.8)$ mm. At this location the mean vorticity was estimated to be approximately 1200/s which compares well with typical VGJs tested⁵ at 15 m/s. The size and location of the vortex shown by the quantitative data of Fig. 17 correspond well with the flow visualization shown in Fig. 5 which was taken at the same test conditions.

Velocity profiles at a fixed g_w are presented in Fig. 18 where the horizontal velocity component normalized by its maximum is presented along the y -axis. The velocity profiles follow similar trends. The velocities between the 2 frequency cases compare within 1% at the maximum positive U-location. As discussed previously, the flow regimes are not similar at a fixed g_w . However, the present data indicate that the velocity profiles follow similar trends.

From the velocity data, the vortex width was estimated and is presented in Fig. 19. For each actuator width, b , several g_w were surveyed producing a range of vortex widths for each actuator width. The average distances between U-maxima are represented by the open circles and the range of vortex widths are indicated by the vertical lines. (Note: these lines do *not* represent error bars.) As expected, the vortex width increases with the actuator width. However, a change in the actuator width by a factor of 3.4 increases the vortex width by only 42%. Also, estimating the vortex size directly from the flow visualization showed the vortex width to be much larger. Thus, the vortex widths of Fig. 19 represent minimum widths.

The vortex flow operational range is presented in Fig. 20. The upper line indicates an unsteady flow regime and the lower line indicates steady flow regimes (free jet and wall jet). The quantity, af , represents the input strength of the actuator to the system. Larger af values correspond to larger actuator velocities producing potentially stronger vortices from the flow control actuator system. As the actuator width is decreased, the range of af values increases. Assuming the vortex strength is not too weak as the actuator size decreases, the larger operational range is advantageous from a design perspective. Overall, to design the flow control actuator to produce a vortex, the scaling presented in Fig. 20 along with the actuator amplitudes (or frequencies) is sufficient.

The vortex flow velocity in the horizontal direction is presented in Fig. 21. The ordinate is the maximum

measured horizontal velocity component at $x=1$ mm measured from $y=0$ to 6.56 mm; the abscissa is the theoretical vertical velocity component at the wide gap. The horizontal velocity increases linearly with velocity input but the rate of increase is small. If all the vertical flow energy at the wide gap is transformed to horizontal flow energy within the vortex then the plotted slope would be 45° degrees. However, the actual slope is 22° since energy is also transformed vertically and to the external flow surrounding the vortex.

The Stokes number scaling is illustrated in Fig. 22. An indication of the actuator efficiency is presented along the y -axis which represents the ratio of the maximum horizontal vortex flow velocity to the theoretical vertical jet velocity from the wide gap. The efficiency varies rapidly for $St < 8$. The maximum efficiency, 0.52, occurs at approximately $St=8$ and then falls off gradually. Following a similar analysis as Rathnasingham et al¹⁹ for the present actuator system, the optimum Stokes number for the vortex flow is 9.66 comparing within 18% of the experimental value.

Concluding Remarks

An oscillatory flow control actuator was characterized in still air using flow visualization and mean velocity measurements. The actuator produces flow in several regimes that may be used for active flow control. The significant conclusions are summarized as follows:

1. The oscillatory flow control actuator generates 3 primary flow regimes (wall jet, free jet, vortex flow) depending on scaled amplitude, actuator Reynolds number, and gap spacing. The primary wall jet represents horizontal flow from the wide to narrow gap near the actuator surface. The primary free jet represents a vertical jet emanating from the wide gap. Finally, the vortex flow represents a flow dominated by a vortex that emanates from the wide gap and extends at least one third the actuator width in diameter.
2. The scaled amplitude range for the wide gap free jet occurs at larger value relative to the scaled amplitude range for the narrow gap free jet. This value is predicted by the Stokes number scaling.
3. The flow control actuator, operated in the vortex flow mode, produces vorticity levels comparable to vortex generator jets.
4. For the range of actuator widths tested, the optimum actuator efficiency occurs at a Stokes number of approximately 8 for the vortex flow. This compares within 18% of the theoretically derived optimum, 9.66.

For the vortex flow field, the actuator operational range increases as the actuator size decreases. This suggests, for the first time that micro-size actuators may provide a larger operational range than macroscopic actuators.

Acknowledgments

This work was performed while the first author held a National Research Council/NASA Langley Research Center Research Associateship. This work was supported under the Aircraft Morphing Program of the NASA

Airframe Systems Program Office. The authors gratefully acknowledge their collaboration with Drs. N. Mansour and P. Koumoutsakos of NASA-Ames, who have provided much insight into the characteristics of these actuators.

References

- ¹Bragg, M.B. and Gregorek, G.M., "Experimental Study of Airfoil Performance with Vortex Generators," *J. Aircraft*, Vol. 24, No. 5, May 1987, pp. 305-309.
- ²Kehro, M., Hutcherson, S., Lieback, R., "Vortex Generators Used to Control Laminar Separation Bubbles," AIAA 90-0051, Jan. 1990.
- ³Lin, J.C., Robinson, S.K., McGhee, R.J., and Valarezo, W.O., "Separation Control on High-Lift Airfoils via Micro-Vortex Generators," *Journal of Aircraft*, Vol. 31, No. 6, 1994, pp. 1317-1323.
- ⁴Johnston, J. and Nishi, M., "Vortex Generator Jets-A Means for Passive and Active Control of Boundary Layer Separation," AIAA 89-0564, Jan. 1989.
- ⁵Compton, D.A. and Johnston, J.P., "Streamwise Vortex Production by Pitched and Skewed Jets in a Turbulent Boundary Layer," AIAA 91-0038, Jan. 1991.
- ⁶McManus, K.R., Joshi, P.B., and Legner, H.H., "Pulsed Vortex Generator Jets for Active Control of Flow Separation," AIAA 94-2218, June 1994.
- ⁷McManus, K.R., Joshi, P.B., Legner, H.H., Davis, S.J., "Active Control of Aerodynamic Stall Using Pulsed Jet Actuators," AIAA 95-2187, June 1995.
- ⁸Seifert, A., Bachar, T., Koss, D., Shepshelovich, M., and Wagnanski, I., "Oscillatory Blowing: A Tool to Delay Boundary-Layer Separation," *AIAA J.*, Vol. 31, No. 11, Nov. 1993, pp. 2052-2060.
- ⁹Seifert, A., Darabi, A., and Wagnanski, I., "Delay of Airfoil Stall by Periodic Excitation," *J. of Aircraft*, Vol. 33, No. 4, July-August 1996, pp. 691-698.
- ¹⁰Gad-El-Hak, M., and Bushnell, D.M., "Separation Control: Review", *J. Fluid Eng.*, Vol. 113, pp. 5-30.
- ¹¹Kibens, V., Parekh, D.E., Bingaman, D.C., Glezer, A., Mossman, M.F., and Rogers, C.B., "Innovative Jet Flow Control - Technology Transfer Process," AIAA 96-0307, Jan. 1996.
- ¹²Wiltse, J.M. and Glezer, A., "Manipulation of free shear flows using piezoelectric actuators," *J. Fluid. Mech.*, Vol. 249, 1993, pp. 261-285.
- ¹³Horner, G.C., "Smart Materials and Structures at NASA LaRC," Proceedings of the 4th Annual NASA LaRC *Advances in Smart Materials for Aerospace Applications Workshop*, May, 1995.
- ¹⁴Jacobson, S.C. and Reynolds, W.C., "An Experimental Investigation Towards the Active Control of Turbulent Boundary Layers," AFSOR Report Number TF-64, March 1995.
- ¹⁵Saddoughi, S.G., "Experimental investigations of on-demand vortex-generators", *Center for Turbulence Research, Annual Research Briefs*, 1994, pp. 197-203.
- ¹⁶Koumoutsakos, P., "Direct numerical simulations of "on-demand" vortex generators - Mathematical formulation," *Center for Turbulence Research, Annual Research Briefs*, 1994, pp. 205-214.
- ¹⁷Koumoutsakos, P., "Simulations of vortex generators," *Center for Turbulence Research, Annual Research Briefs*, 1995, pp. 233-240.
- ¹⁸Panton, R.L., *Incompressible Flow*, John-Wiley & Sons, New York, 1984.
- ¹⁹Rathnasingham, R. and Breuer, K.S., "Characteristics of Resonant Actuators for Flow Control," AIAA 96-0311, Jan. 1996.

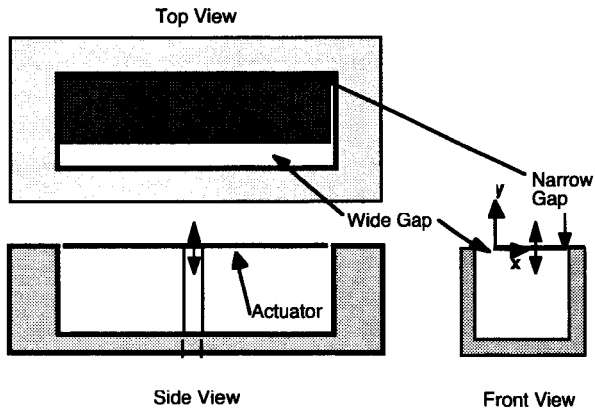


Figure 1. Flow control actuator

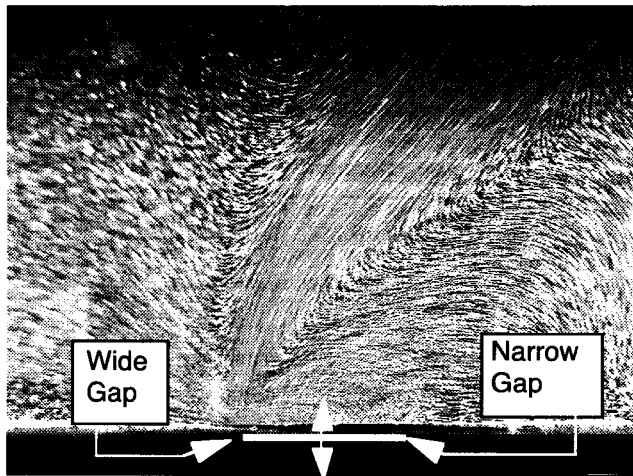


Figure 2. Angled jet at wide gap: $f=70$ Hz, $g_r=3$, $S_a=0.13$, $Re=56$

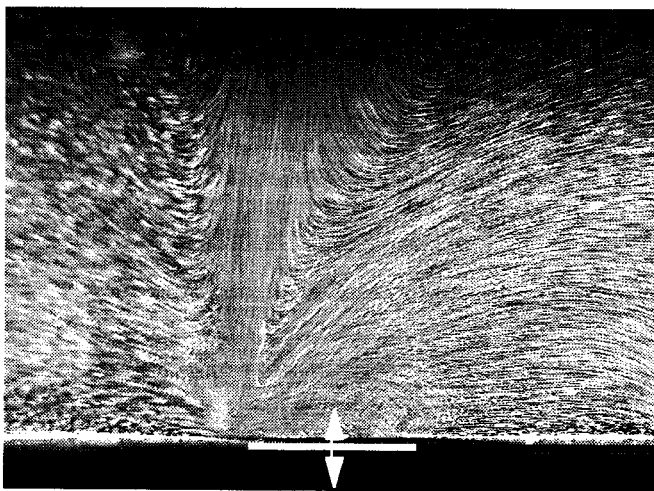


Figure 3. Jet at wide gap: $f=70$ Hz, $g_r=3$, $S_a=0.19$, $Re=80$

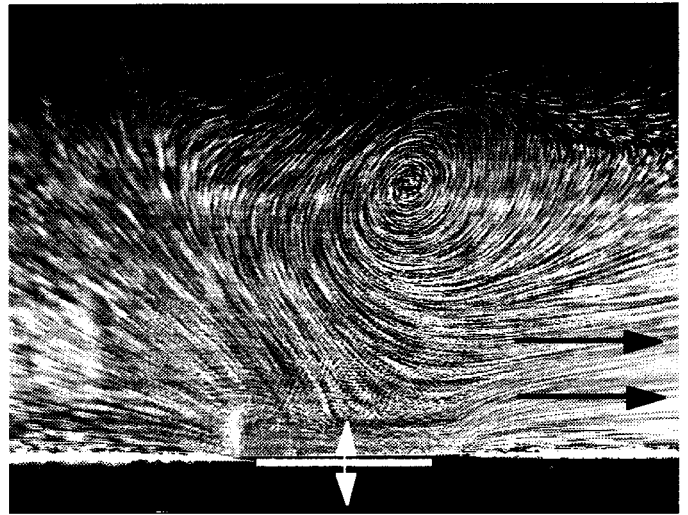


Figure 4. Horizontal flow: $f=210$ Hz, $g_r=3$, $S_a=0.11$, $Re=134$

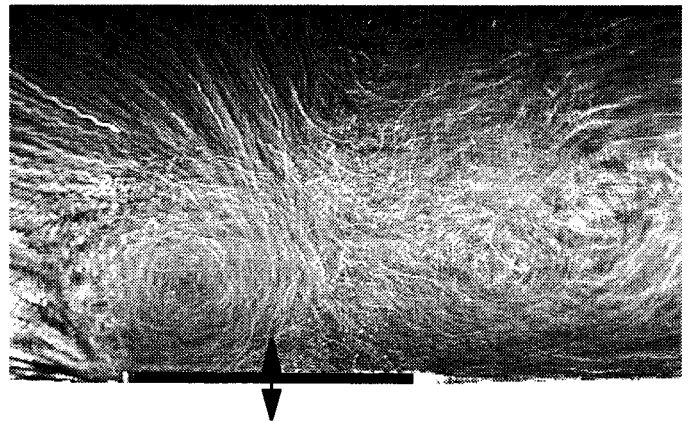


Figure 5. Vortex flow: $f=190$ Hz, $g_r=3$, $S_a=0.13$, $Re=146$

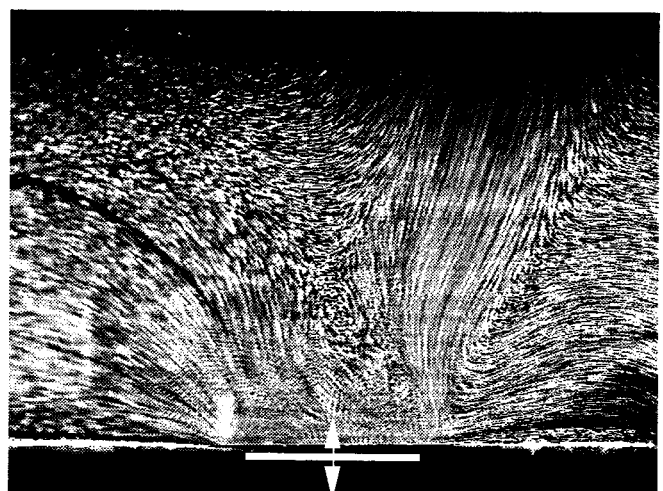


Figure 6. Jet at narrow gap: $f=150$ Hz, $g_r=5$, $S_a=0.14$, $Re=124$

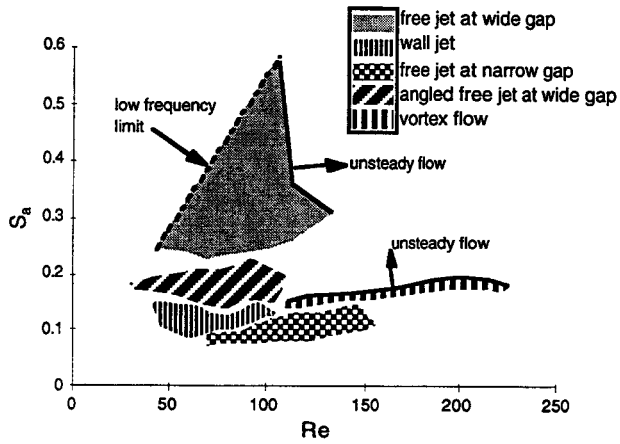


Fig. 7. Non-dimensional scaling: $g_r=1$ ($b=9.65$ mm)

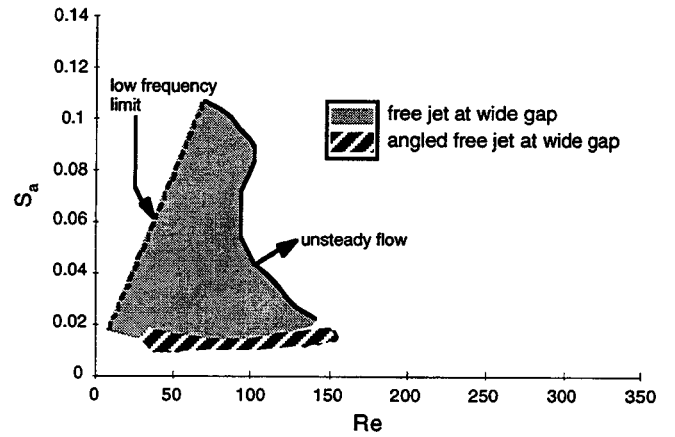


Figure 10. Non-dimensional scaling: $g_r=1$ ($b=18.8$ mm)

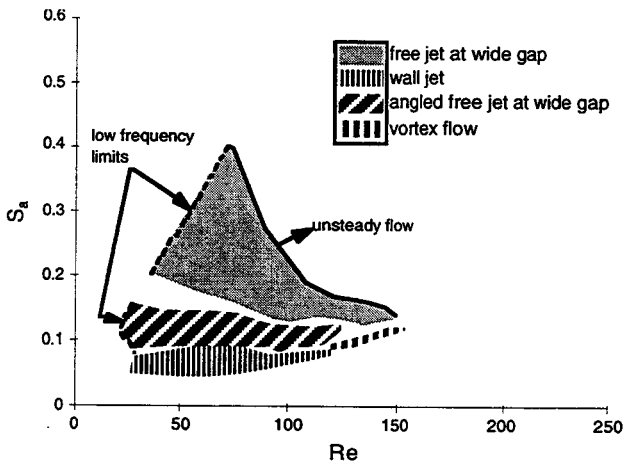


Fig. 8. Non-dimensional scaling: $g_r=2$ ($b=9.65$ mm)

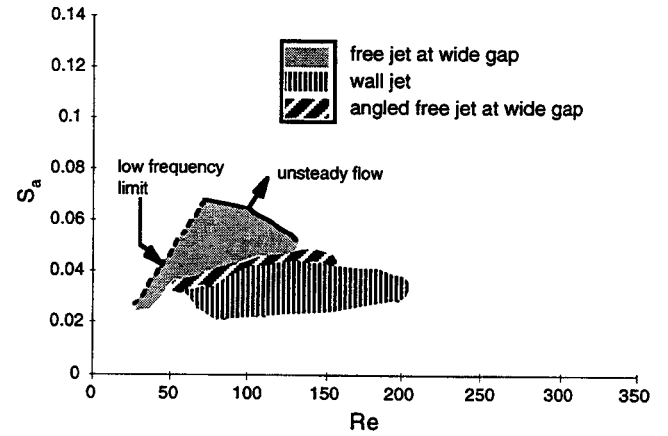


Figure 11. Non-dimensional scaling: $g_r=2$ ($b=18.8$ mm)

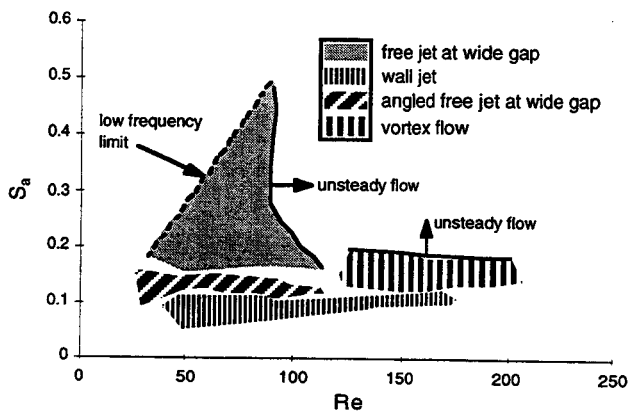


Fig. 9. Non-dimensional scaling: $g_r=3$ ($b=9.65$ mm)

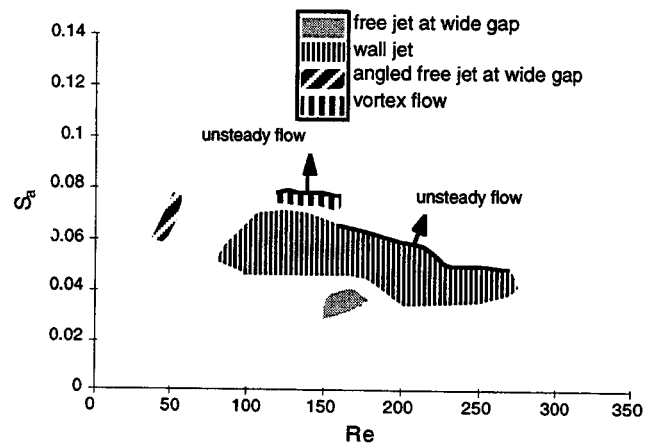


Figure 12. Non-dimensional scaling: $g_r=3$ ($b=18.8$ mm)

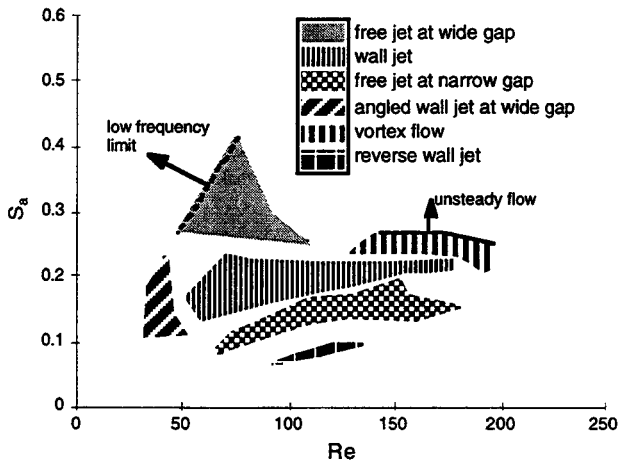


Figure 13. Non-dimensional scaling: $g_r=5$ ($b=9.65$ mm)

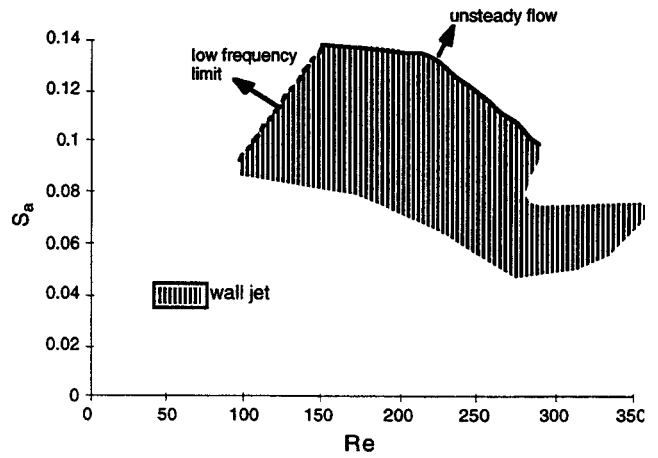


Figure 16. Non-dimensional scaling: $g_r=5$ ($b=18.8$ mm)

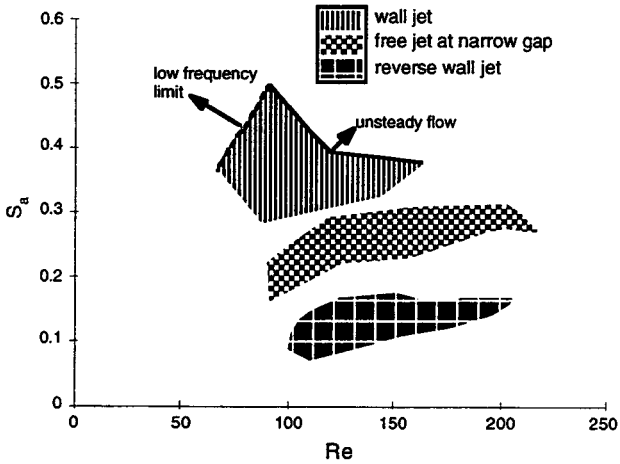


Figure 14. Non-dimensional scaling: $g_r=8$ ($b=9.65$ mm)

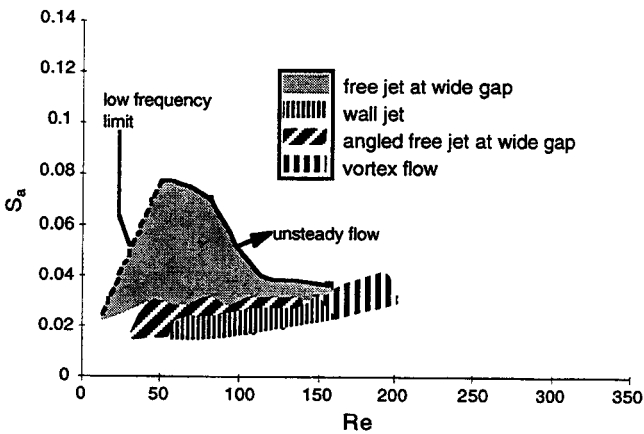


Figure 15. Non-dimensional scaling: $g_r=1.5$ ($b=18.8$ mm)

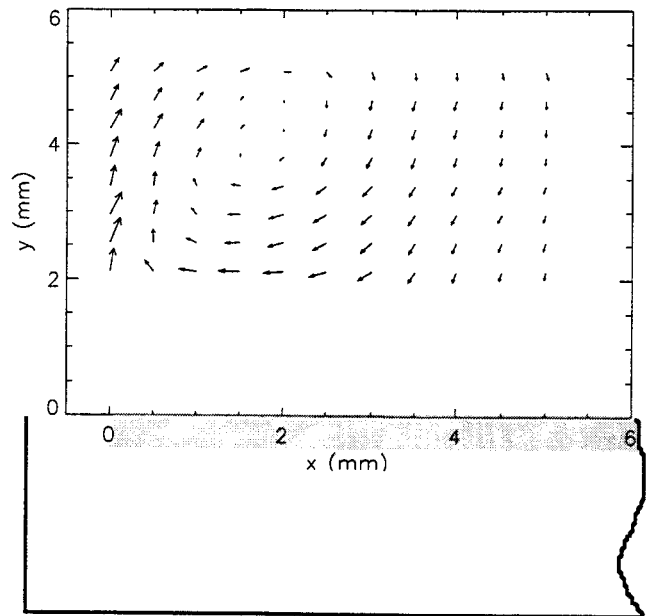


Figure 17. Vortex flow velocity vectors: $f=190$ Hz, $g_w = 0.0998$ ($b=9.65$ mm), $S_a = 0.13$, $Re=146$

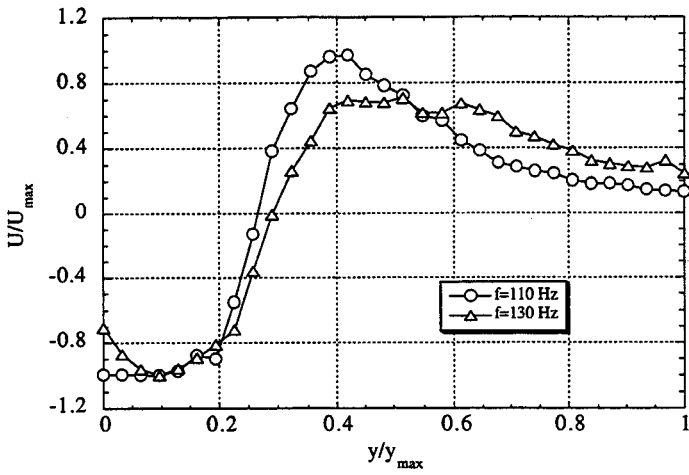


Figure 18. Velocity profiles at $x=1$ mm, $g_r=3.75$

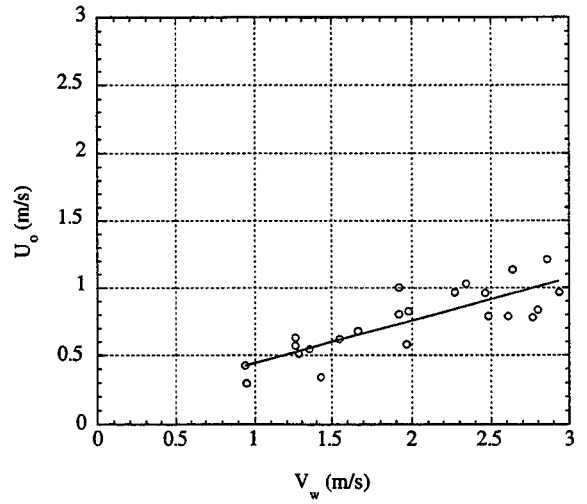


Figure 21. Horizontal velocity as a function of theoretical velocity at the wide gap

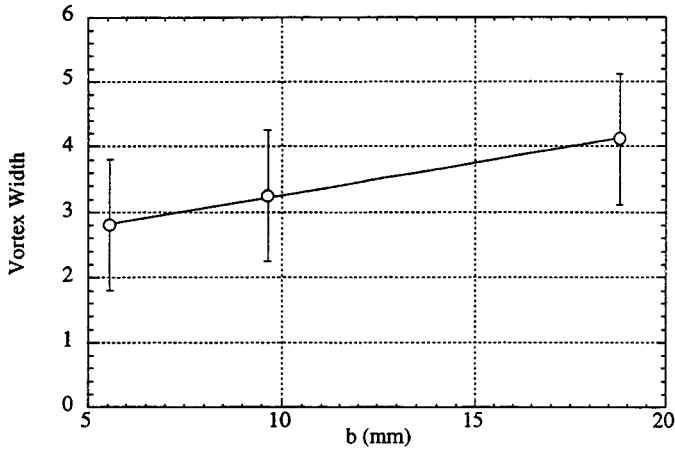


Figure 19. Scaling of vortex width with actuator width

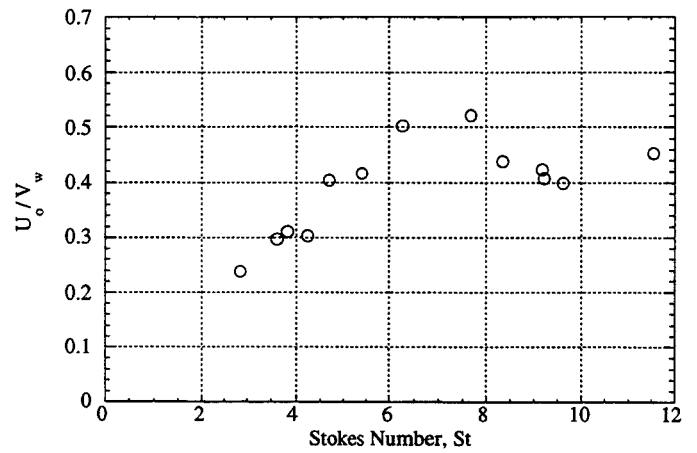


Figure 22. Stokes number scaling

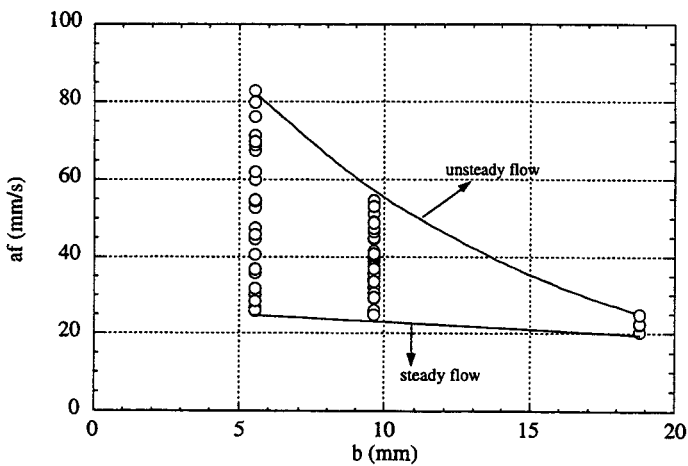


Figure 20. Vortex flow operational range